CHAPTER 4

ISOLATING THE EROSIVITY AND ERODIBILITY COMPONENTS IN EROSION BY RAIN-IMPACTED FLOW

As noted in Chapter 2, Meyer (1981) and Foster (1982) observed that the rate sediment is transported across a unit width of the boundary between a ridge and a furrow was empirically related to R^2 (Eq. 2.2 with w=2). They also identified the need to distinguish between erosion that occurs in rills, which is largely driven by flow energy, and erosion that occurs in the interrill areas, which is largely driven by raindrop energy. Although Meyer stated that soil erosion in interrill areas combines the processes of detachment by raindrop impact, transport by splash, and transport by very thin flow, he did not study these various processes or attempt to account for their contribution to interrill erosion in his experiments. The current understanding is that transport by thin flow is the major transport mechanism in interrill areas (Elliot *et al.*, 1991).

It was shown in Chapter 2 that, although the coefficient K in Eq. 2.2 was influenced by soil properties, because other factors influenced it, it was not a fundamental soil property in any sense. In contrast, the coefficient k_s in Eq. 3.28 provides a better measure of the susceptibility of the surface to erosion by rain-impacted flow because other terms account for the factor influencing the erosiveness of rain-impacted flow. Unfortunately, flow depth is usually unknown is most laboratory and field experiments so that Eqs. 3.25 - 3.29 cannot be used directly in practical predictive models for interrill erosion. However, Eq. 3.28 does provide a basis for an empirical model in which the "soil" factor may be more directly related to soil properties.

4.1 ALTERNATIVE INTERRILL ERODIBILITIES FOR CROPLAND SOILS IN THE USA

4.1.1 An alternative practical model for interrill erosion

Liebenow *et al.* (1990) presented an analysis of the interrill erodibilities for 18 cropland soils in the USA based on the equation

$$D_i = K_i R^2 S_f \qquad (4.1)$$

where D_i is the interrill erosion rate, K_i is the interrill erodibility, R is the intensity of the rainfall, and S_f is a slope factor. Liebenow *et al.* observed that

$$S_f = 1.05 - 0.85 \exp\{-4 \sin(\phi)\} \quad (4.2)$$

where ϕ is the slope angle. The analysis was done on data collected as part of the Water Erosion Prediction Project (WEPP). These data are reported in detail in Elliot *et al.* (1989). Because shallow rain-impacted flow dominates the transport of soil material in the type of experiment used by Liebenow *et al.*

$$D_i = q_{sR} L_x^{-1} \quad (4.3)$$

where L_x is the length of the eroding surface in the downstream direction. It follows from Eqs. 4.1 - 4.3 that

$$K_i = \frac{q_{sR}}{L_x R^2 [1 - 0.85 \exp\{-4 \sin(\phi)\}]} \quad (4.4).$$

Table 4.1 shows the values of K_i calculated from the runoff and sediment concentration data of Elliot *et al.* for the 18 soils used by Liebenow *et al.* using Eq. 4.4 and

$$q_{sR} = q_w c_R \quad (4.5)$$

where, as defined previously, q_w is the rate water is discharged across a unit width of any arbitrary boundary and c_R is the sediment concentration resulting from the raindrops impacting the flow. These values are identical to those given by Liebenow *et al.*.

It follows from Eq. 4.5 that c_R can be calculated by dividing q_{sR} by q_w. As shown by Eq. 2.21, q_w is given by the product of flow depth (h) and velocity (u). Thus, it follows from Eqs. 3.12 and 2.21 that

$$c_R[s,r] = k_s R f[h,r] h^{-1} \quad (4.6)$$

and, from Eqs. 4.5 and 4.6,

Table.4.1. Values of K_i and their coefficients of variation (CV) obtained using Eqs. 4.4 and 4.5 with the data of Elliot *et al.* (1989) for the soils used by Liebenow *et al.* (1990). The soils are ordered according to the most precise (underlined) estimates of K_i ($K_i$best).

	FLAT PLOTS		ALL PLOTS	
	$K_i x10^{-6}$ (kg.s.m^{-4})	CV (%)	$K_i x10^{-6}$ (kg.s.m^{-4})	CV (%)
Palouse	5.26	44.35	4.32	32.90
Amarillo	3.83	45.69	4.12	33.37
Williams	3.69	4.06	2.94	23.12
Keith	3.25	31.80	3.37	24.44
Hersh	3.26	22.51	3.93	34.23
Zahl	2.91	1.37	3.18	24.56
Nansene	2.85	18.25	3.12	20.97
Los Banos	2.78	5.57	2.50	12.81
Whitney	2.06	39.76	2.74	32.12
Hieden	2.59	27.17	1.70	42.75
Academy	2.54	3.34	2.89	22.11
Woodward	2.19	4.78	4.00	36.32
Sharpsberg	1.65	27.27	1.86	23.69
Pierre	1.83	6.01	2.18	17.24
Barnes-ND	1.20	23.65	1.71	21.11
Barnes-MN	1.88	29.79	1.60	25.94
Sverdrup	1.33	18.36	2.11	26.96
Portneuf	0.88	30.68	1.26	25.03
Mean CV		21.4		26.6

$$q_{sR} = k_s\, q_w\, R\, f[h,r]\, h^{-1} \qquad (4.7)$$

Although a direct influence of R on c_R is evident in Eq. 4.6, R influences q_w and hence h. Experiments by Mutchler and McGregor (1983) suggest that $f[h,r]$ for a rain with a non-uniform drop-size distribution peaks when h is about 2mm. The analysis of data from laboratory experiments confirms this (Fig. 3.26) but, as shown in Fig. 4.1, the term $f[h,r]h^{-1}$, and hence c_R, for rain tends to decrease exponentially with flow depth when h is less than about 5mm. Despite this, as shown in Figs. 2.4 and 2.5, linear intensity - sediment concentration relationships have been observed in the experiments of Walker *et al.* (1978), where L_x was 3m, and Meyer and Harmon (1989), where L_x was 150mm to 600mm. Evidently, in these experiments, the direct effect of variations in drop impact frequency on c_R was sufficient to mask any effect variations in R may have had on h. This is likely to be common in most experiments involving shallow rain-impacted flows.

It is well known that slope gradient affects flow depth and velocity. Although, when flow velocities are not sufficient for the flow to entrain soil material without the aid of raindrop impact, c_R varies independently of u (Eq. 4.6), a factor accounting for the effect of slope gradient on c_R through h has to be taken into account in modelling interrill erosion. Thus it follows from Eq. 4.7 that

$$q_{sR} = k_1\, q_w\, R\, f[S] \qquad (4.8)$$

where $f[S]$ is a function accounting for the effect of slope gradient on q_{sR}, and k_1 is a coefficient influenced by variations in soil characteristics and also by variations in flow depth that are not accounted for directly by $f[S]$. As shown by Fig. 4.2,

$$f[S] = S \qquad (4.9)$$

results from an analysis of the data of Meyer and Harmon (1989). Figure 4.2 also shows that, although slope length is one of the factors that can be expected to affect k_1, provided they are within reasonable limits, variations slope length can be ignored. Under these circumstances, Eq. 4.8 becomes

$$q_{sR} = k_1\, q_w\, R\, S \qquad (4.10)$$

FIG. 4.1

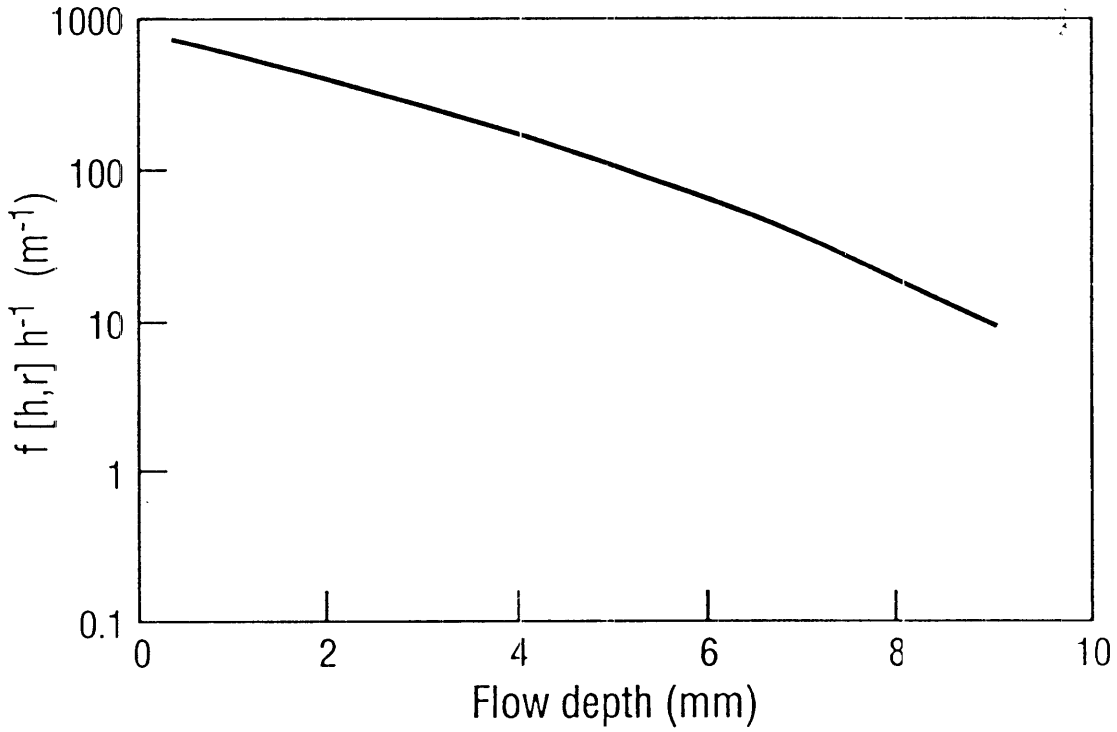

Figure 4.1

Figure 4.1. The relationship between flow depth and $f[h,r]h^{-1}$ that results from the data given in Fig.3.26A.

FIG. 4.2

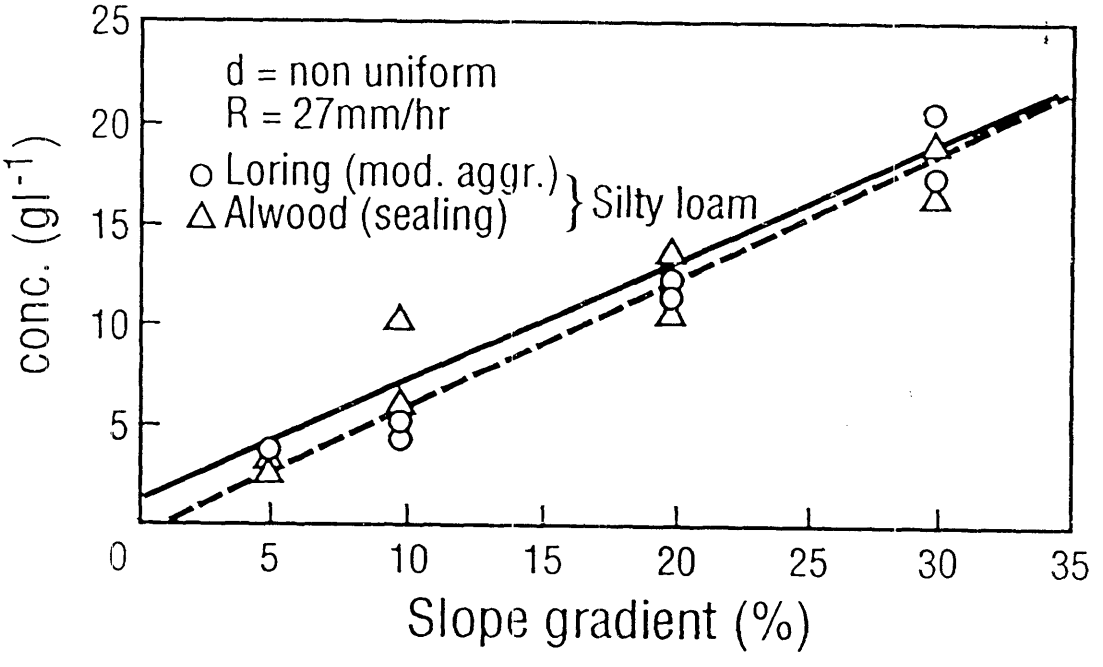

Figure 4.2. The effect of slope gradient on sediment concentrations in experiments by Meyer and Harmon (1989) with 600mm long slopes.

In the experiments analysed by Liebenow *et al.* (1990), 10 interrill plots were used. Of these, 6 were "ridged" plots. These plots had 250 mm long sideslopes with gradients of about 50 %. In the remaining four, the ridges were smoothed out to give "flat" plots. These plots had 750 mm long slopes with gradients of 3 to 6 %. In the Meyer and Harmon (1989) experiments, 5 % $\leq S \leq$ 30 % and slope lengths were 150 to 600 mm. Consequently, Eq. 4.10 is likely to be valid for the flat plots. Thus, for these plots,

$$k_1 = \frac{q_{sR}}{Rq_w S} \qquad (4.11)$$

However, it should be noted that this equation should not be used at very low slope gradients. For S=0, Eq. 4.10 indicates c_R=0 but, when S=0, flow can still occur and the flow can be shallow enough for c_R>0.

Equation 4.10 may also not be applicable at high slope gradients. In their analysis of the slope effect, Liebenow *et al.* present data that indicate c_R will be overpredicted by extrapolating Eq. 4.9 to the slope gradients used in the ridged plots. Thus Eq. 4.10 has to be modified to

$$q_{sR} = k_1 \, Rq_w S \, f_s \qquad (4.12)$$

where f_s=1.0 for the flat plots and f_s<1.0 for the ridged plots. Rearranging Eq. 4.12 gives

$$f_s = \frac{q_{sR}}{k_1 RSq_w} \qquad (4.13)$$

and, because k_1 can be assumed to be a constant for any given soil, the values of f_s for the ridged plots can be determined from this equation by using the values of k_1 determined by applying Eq. 4.11 to the data from the flat plots.

4.1.2 Alternative interrill erodibilities for 18 cropland soils

Table 4.2 shows the values of k_1 calculated for the flat plots by applying Eq. 4.11 to the data of Elliot *et al.* (1989) used by Liebenow *et al.*

Table.4.2. Values of k_1 and their coefficients of variation (CV) obtained using Eqs. 4.5 and 4.12 on the data of Elliot *et al.* (1989) for the soils used by Liebenow *et al.* (1990). The values of k_1 are based on conventional units for c(g l^{-1}), R(mm h^{-1}) and S(%). The soils are ordered according to the most precise (underlined) estimates of k_1 ($k_1$best).

SOIL	FLAT PLOTS		ALL PLOTS	
	$k_1 x10^{-3}$ ($s.m^{-1}$)	CV (%)	$k_1 x10^{-3}$ ($s.m^{-1}$)	CV (%)
Amarillo	<u>47.95</u>	26.00	32.26	45.84
Williams	<u>36.50</u>	6.31	22.72	42.67
Los Banos	<u>32.87</u>	0.50	23.18	29.34
Palouse	39.24	32.43	<u>32.80</u>	25.93
Sharpsberg	<u>29.66</u>	16.58	18.47	38.03
Nansene	26.82	23.37	<u>28.26</u>	17.49
Heiden	<u>27.32</u>	13.51	13.54	68.63
Academy	<u>26.64</u>	0.82	22.61	16.65
Keith	27.18	32.23	26.06	24.75
Hersh	<u>23.44</u>	13.81	35.75	33.90
Zahl	<u>23.15</u>	2.10	21.31	16.20
Sverdrup	14.18	36.02	<u>12.02</u>	25.80
Woodward	<u>17.14</u>	4.69	30.96	31.54
Pierre	<u>16.81</u>	7.07	16.27	7.09
Barnes-MN	15.37	25.34	<u>15.23</u>	20.63
Whitney	13.68	31.96	<u>14.44</u>	29.44
Barnes-ND	<u>12.96</u>	7.26	15.52	15.70
Portneuf	<u>11.84</u>	9.56	10.08	22.76
Mean CV		16.09		28.47

(1990). Fig. 4.3 shows the result of using these values to determine f_s for the ridged plots. Regression analysis performed on this data set indicates that

$$f_s = 0.259 + 0.000049\ (1.197^{[90-S]}) \qquad \text{for } S>38\% \qquad (4.14)$$

provides a reasonable approximation of the f_s to S relationship for the ridged plots. However Eq. 4.14 accounts for only 28.5% of the variation in f_s for S>38 %. As a result of this, the precision by which k_1 can be estimated was enhanced in only one third of soils through the inclusion of the ridged condition (Table.4.2). Only in the case of two soils did the enhanced precision indicate any substantial change from the ranking of the soils obtained from the values of k_1 for the flat plots. In comparison, the precision by which K_i can be estimated from Eq. 4.4 was enhanced by including the ridged plots in almost half of the soils (Table.4.1).

Figure 4.4 provides a comparison of the rankings provided by k_1 and K_i for the 18 soils being considered here. From the coefficients of variation (CV) shown in Tables 4.1 and 4.2, the k_1 values obtained on the flat plots provided, on average, the most accurate means of accounting for the differences between the soils considered by Liebenow *et al.*. k_1 is linearly related to K_i (Fig. 4.5) but k_1 values for about one third of the soils are not likely to be predicted within ±20 % from K_i. Also, Table 4.3 shows that the best estimates of k_1 would give significantly different indications of the susceptibilities of some soils to interrill erosion than those obtained using K_i.

4.1.3 Discussion

Figure 4.3 shows that, for S>30%, f_s appears to decline rapidly with increasing slope gradient but then tends to vary little from a value of about 0.3 when S>45 %. A less abrupt change in f_s between the flat and ridged plots was expected. The observation that f_s = 1.0 for S≤30 % results from experiments with plots 150 – 600 mm in length. Thus, with flow paths for rain-impacted flow of 250 mm for the ridged plots and 750 mm for the flat plots, it seems unlikely that slope length is one of the factors responsible for the

FIG. 4.3

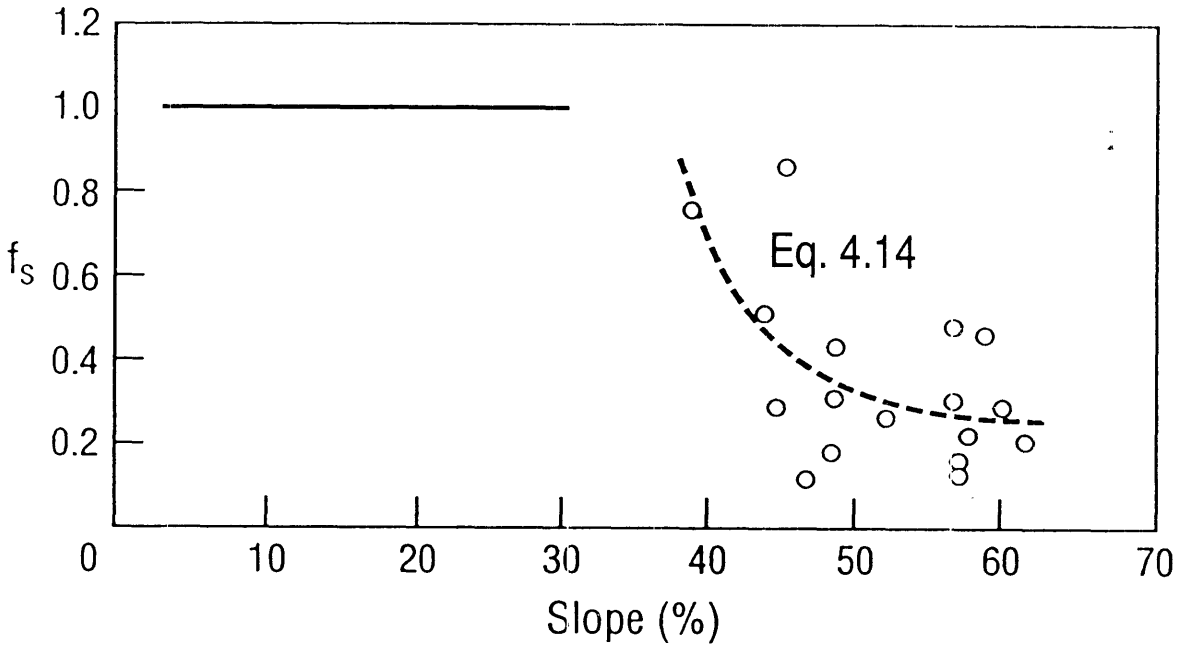

Figure 4.3. The relationship between f_s and slope gradient for the 18 soils examined by Liebenow *et al.* (1990).

Soil Relative susceptibility to interill erosion

FIG. 4.4

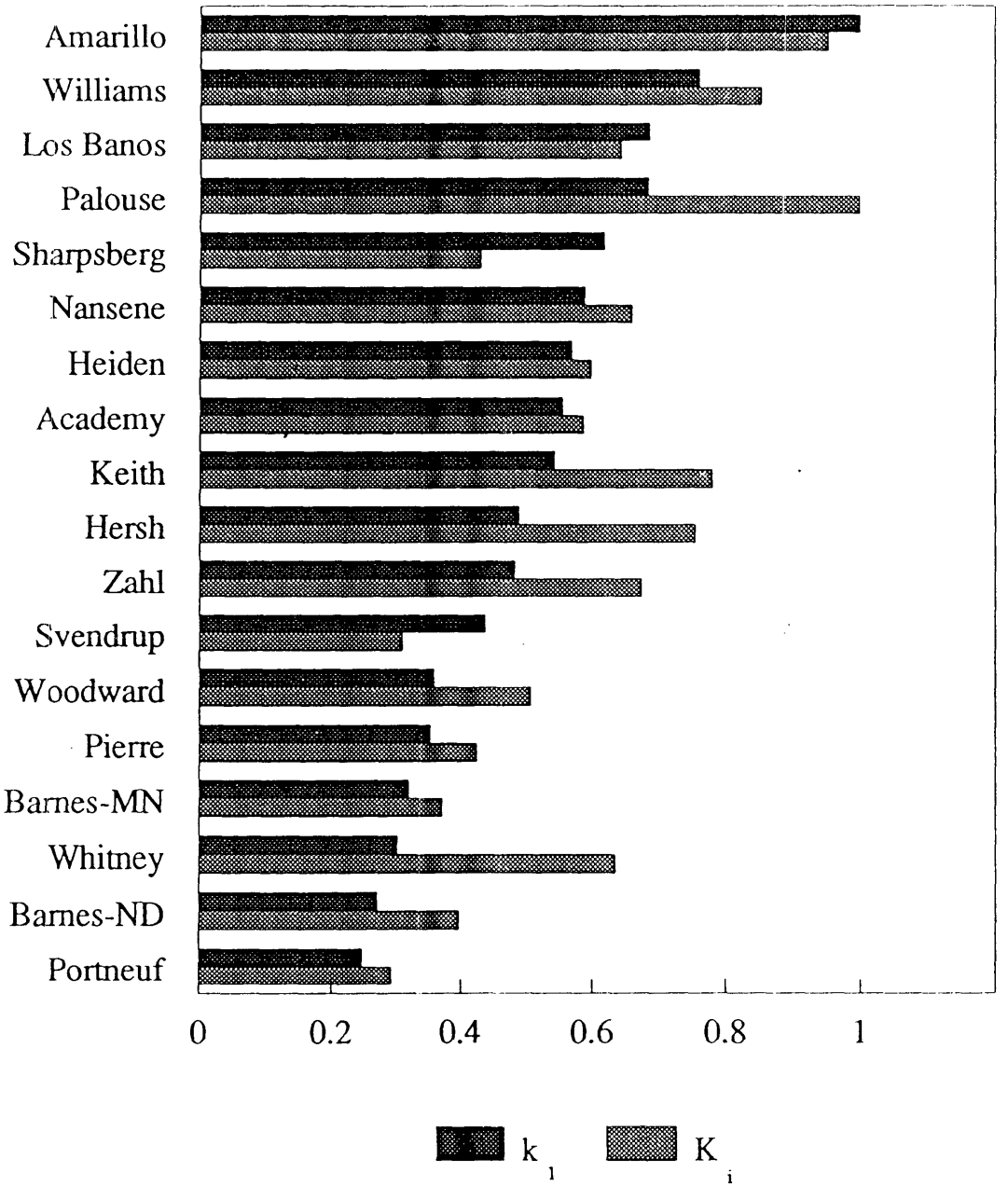

Figure 4.4. Bargraph of the relative values of $k_1$best and $K_i$best for the 18 soils considered in Tables 4.1 and 4.2. The values shown for each parameter are scaled so that a value of 1.0 is allocated to the maximum.

FIG. 4.5

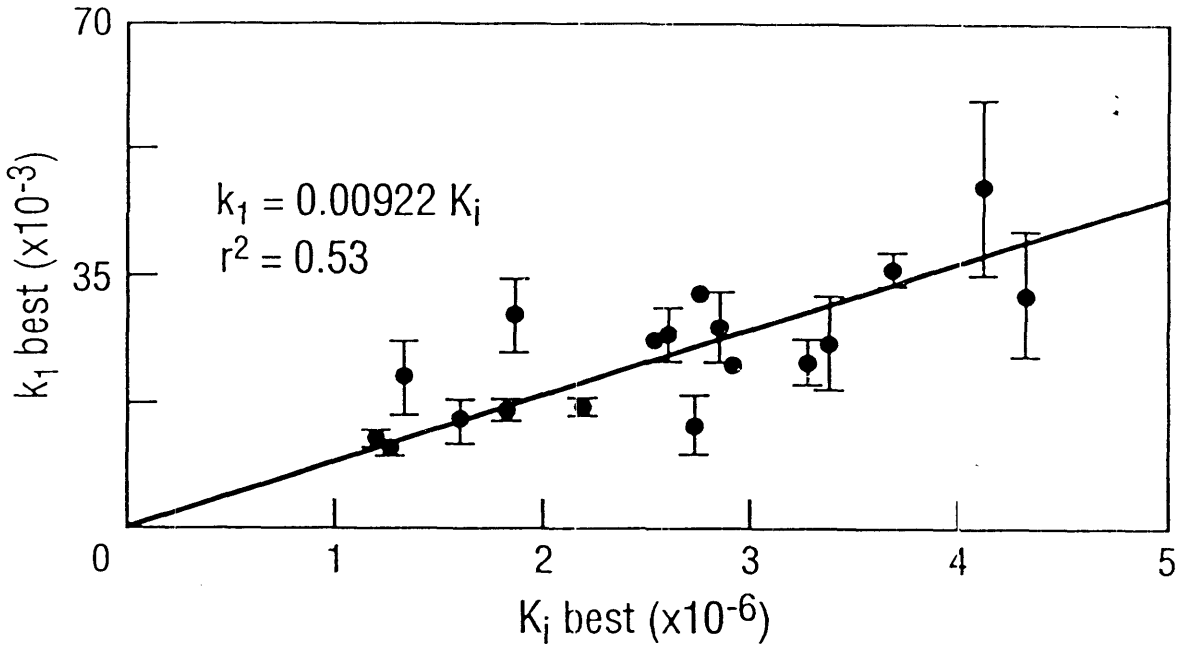

Figure 4.5. The relationship between $k_1$best and $K_i$best for the data given in Tables 4.1 and 4.2.

Table 4.3. Matrix for significant differences in k_1 and K_i for the underlined values ($k_1$best, $K_i$best) in Tables 4.1 and 4.2. *s indicate those soils that are significantly different at a 10 % level of probability.

A: Significant difference in $k_1$best at 10% probability

	SOIL	1	2	3	4	5	6	7	8	9	10	11	12	13	14	15	16	17	18
1	Sharpsberg	-	-	-	-	-	-	*	-	-	*	-	-	-	-	-	*	-	*
2	Hersh	-	-	-	-	-	-	*	-	-	*	-	-	-	-	*	*	-	*
3	Keith	-	-	-	*	-	-	*	-	-	*	-	-	-	-	*	*	-	*
4	Amarillo	-	-	*	-	-	-	*	-	-	-	*	-	-	-	-	-	*	*
5	Woodward	-	-	-	-	-	-	-	*	*	*	*	*	*	-	*	*	-	-
6	Heiden	-	-	-	-	-	-	*	-	-	*	-	-	-	-	-	*	-	*
7	Whitney	*	*	*	*	-	*	-	*	*	-	*	*	*	-	*	-	*	-
8	Academy	-	-	-	-	*	-	*	-	*	*	-	-	*	*	*	*	-	*
9	Los Banos	-	-	-	-	*	-	*	*	-	*	-	-	*	*	-	*	*	*
10	Portneuf	*	*	*	-	*	*	-	*	*	-	*	*	*	*	*	-	*	-
11	Nansene	-	-	-	*	*	-	*	-	-	*	-	-	-	*	*	*	*	*
12	Palouse	-	-	-	-	*	-	*	-	-	*	-	-	-	*	-	*	*	*
13	Zahl	-	-	-	-	*	-	*	*	*	*	-	-	-	*	*	*	-	*
14	Pierre	-	-	-	-	-	-	-	*	*	*	*	*	*	-	*	-	-	-
15	Williams	-	*	*	-	*	-	*	*	-	*	*	-	*	*	-	*	*	*
16	Barnes-ND	*	*	*	-	*	*	-	*	*	-	*	*	*	-	*	-	-	-
17	Sverdrup	-	-	-	*	-	-	*	-	*	*	*	*	-	-	*	-	-	*
18	Barnes-MN	*	*	*	*	-	*	-	*	*	-	*	*	*	-	*	-	*	-

B: Significant difference in $K_i$best at 10% probability

	SOIL	1	2	3	4	5	6	7	8	9	10	11	12	13	14	15	16	17	18
1	Sharpsberg	-	*	*	*	-	-	*	-	*	*	*	*	*	-	*	-	-	-
2	Hersh	*	-	-	-	-	-	-	-	-	*	-	-	-	-	-	*	-	*
3	Keith	*	-	-	-	-	-	-	-	-	*	-	-	-	*	-	*	*	*
4	Amarillo	*	-	-	-	-	-	*	-	-	*	-	-	-	*	-	*	*	*
5	Woodward	-	-	-	-	-	-	-	-	*	*	-	-	*	-	*	-	*	-
6	Hieden	-	-	-	-	-	-	-	-	-	*	-	-	-	-	-	*	-	*
7	Whitney	*	-	-	*	-	-	-	-	-	*	-	*	-	-	-	*	-	*
8	Academy	-	-	-	-	-	-	-	-	-	*	-	-	*	*	*	*	*	*
9	Los Banos	*	-	-	-	*	-	-	-	-	*	-	-	-	*	*	*	*	*
10	Portneuf	*	*	*	*	*	*	*	*	*	-	*	*	*	*	*	*	-	-
11	Nansene	*	-	-	-	-	-	-	-	-	*	-	-	-	-	-	*	-	*
12	Palouse	*	-	-	-	-	-	*	-	-	*	-	-	-	*	-	*	*	*
13	Zahl	*	-	-	-	*	-	-	*	-	*	-	-	-	*	*	*	*	*
14	Pierre	-	-	*	*	-	-	-	*	*	*	-	*	*	-	*	-	-	-
15	Williams	*	-	-	-	*	-	-	*	*	*	-	-	*	*	-	*	*	*
16	Barnes-ND	-	*	*	*	-	*	*	*	*	*	*	*	*	-	*	-	-	-
17	Sverdrup	-	-	*	*	*	-	-	*	*	-	-	*	*	-	*	-	-	-
18	Barnes-MN	-	*	*	*	-	*	*	*	*	-	*	*	*	-	*	-	-	-

"step change" in f_s seen in Fig. 4.3. On the contrary, from Fig. 4.1 and the fact that Eq. 4.13 can be written as

$$f_s = \frac{c_R}{k_1 RS} \qquad (4.15),$$

f_s would be expected to increase rather than decrease with decreases in slope length. In effect, using Eq. 4.14 in the analysis presented here did little more than increase the number of observations associated with k_1 for each soil. This is because its development was based on the assumption that k_1 did not vary between the flat and the ridged plots. While it may be difficult to identify the exact reason for the discontinuity in f_s observed in Fig. 4.3, it is possible that this particular assumption is a factor contributing to it. With higher flow velocities on the ridged plots, the values of k_s for these plots may have been dominated more by $D_{pd.M}$ (Eq. 2.24) than on the flat plots. This could have resulted in the values of k_1 for the ridged plots being less than the values of k_1 for the flat plots because usually $D_{pd.M}<D_{pd.D}$.

Arguably, because Eqs. 4.10 and 4.12 attempt to account for the effect of flow velocity and the protective effect of flow depth on q_{sR} through q_w and S, k_1 may be more directly related to soil's true susceptibility to erosion by rain-impacted flow than K_i. If this is the case, then there are dangers in neglecting the effect of variations in runoff in determining the susceptibility of soil surfaces to interrill erosion. An analysis of an unrelated experiment illustrates this.

Elwell (1986) eroded a number of 0.75 m long soil surfaces inclined at 4.5 % under a rainfall simulator. The soil surfaces differed in terms of the sizes of the water stable aggregates present and all the surfaces were subjected to a fixed quantity of rainfall kinetic energy (750 J m^{-2}). He found that the amounts of soil (S_L, grams) and runoff (Q, litres) discharged from the surfaces were related to the mean weight diameter (D_{wsa}, millimetres) of the water-stable aggregates by

$$S_L = 277.18 - 149.16D_{wsa} + 19.41D_{wsa}^2 \qquad ,r^2=0.957 \qquad (4.16)$$

and

$$Q = 9.02 + 0.918D_{wsa} - 1.2385D_{wsa}^2 \quad , r^2=0.956 \quad (4.17)$$

In these experiments, 27.3 mm of rain at a rate of 166mm h^{-1} was applied after a pre-treatment of 36.5 mm of rain at the same intensity (Elwell pers com). Under these circumstances, the infiltration rates and runoff rates probably remained relatively constant over the time of the experiment. The values of k_1 that result from using Eq. 4.11 and this assumption are presented in Fig. 4.6.

Now consider the situation if Elwell had applied the same amount of rain but had used an intensity of 62 mm h^{-1}, the nominal rainfall intensity (range 51-86mm h^{-1}) used in the WEPP experiments, and the drop-size characteristics of the rain remained unchanged. Fig. 4.7A shows the result of applying Eq. 4.10 with the k_1 values shown in Fig. 4.6 to this case. The soil losses are considerably lower than obtained with the 166 mm h^{-1} rain despite the surfaces receiving an identical amount of rain energy because, firstly, from Eqs. 4.5 and 4.10, c_R ($=k_1RS$) decreased by 63 % between R=166 mm h^{-1} and R=62 mm h^{-1} and secondly, the runoff amounts (Fig. 4.7B) were substantially less under the 62 mm h^{-1} rainfall despite the increased duration of exposure to rain. This is simply because, under equilibrium conditions, the runoff rate is the difference between the rainfall rate and the infiltration rate, and it has been assumed that the infiltration rates of the soil surfaces have not varied significantly between the two rainfall rates.

The results of the simulation for the 62 mm h^{-1} rain are based on the assumption that k_s, and consequently k_1, has not varied between the two rainfall rates. Now consider the data in Fig. 4.7 in terms of Eq. 4.4. The values of K_i produced by applying this equation to these data are also presented in Fig. 4.6. This figure shows a substantial difference between the values of K_i obtained at the two rainfall rates because Eq. 4.4 is not capable of accounting for the effects of the variations in runoff adequately. It is because Eq. 4.10 is better at doing this that it tends to provide the more accurate means of determining variations in the susceptibility of soil surfaces to interrill erosion in many experiments. This is important when examining the effects of soil properties on soil erodibility. Failure to use models that adequately account for the fundamental soil processes will cause

FIG. 4.6

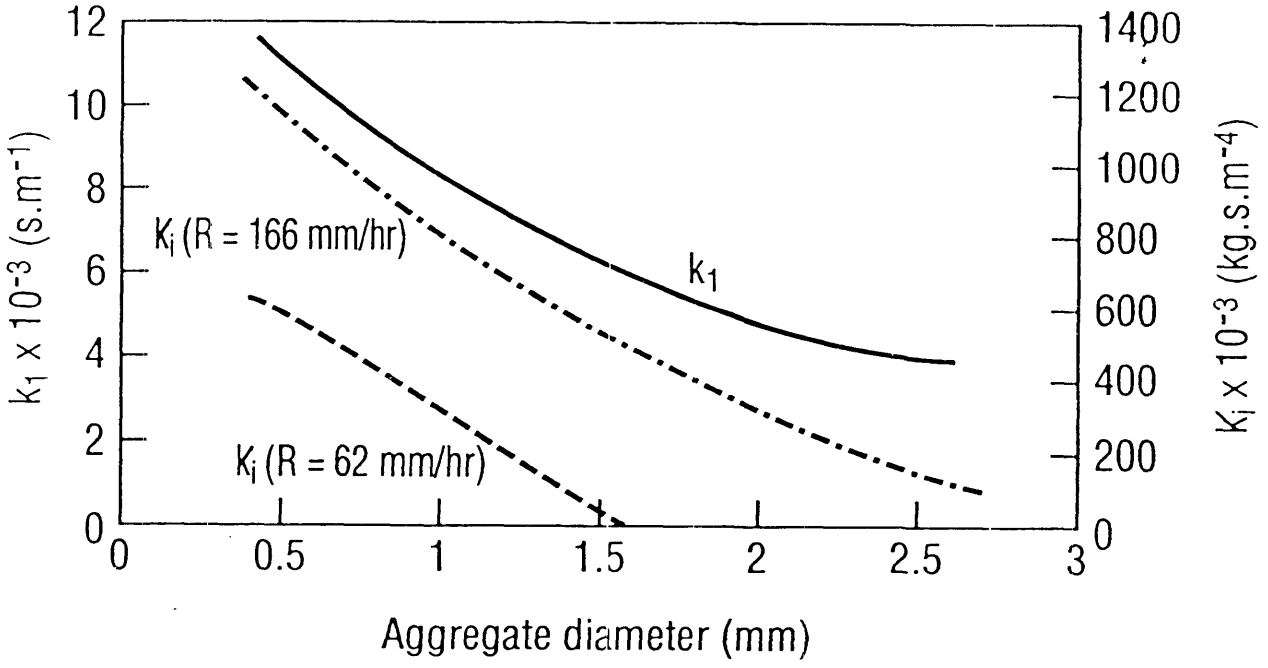

Figure 4.6. k_1 and K_i values calculated for the experiments cf Elwell (1986, R=166 mm h^{-1}) and when R=62 mm h^{-1}.

FIG. 4.7

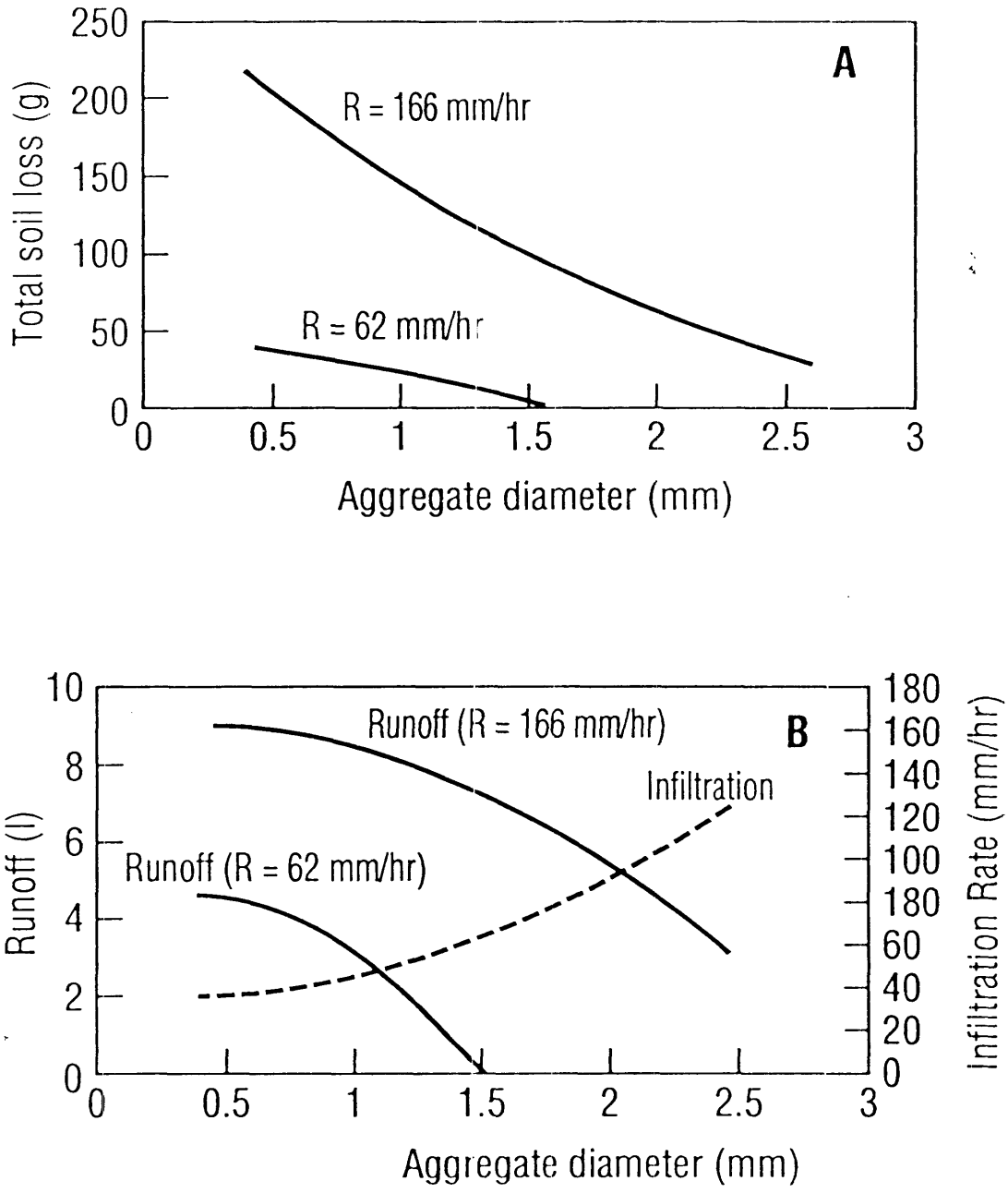

Figure 4.7. Observed and predicted soil losses (A) and runoff volumes (B) for different rainfall intensities under conditions associated the experiments of Elwell (1986).

difficulties in relating measured soil properties to the soil erodibilities determined using these models.

4.2 EROSION UNDER PULSED RAINFALL

In Elwell's experiments, the rain was applied continuously throughout the erosion event. In the experiments that generated the data on which the cropland erodibilities were based, the rain was applied by fan shaped sprays that were swept across the eroding surface. In these particular experiments, a rotating mechanism was used but, in many field rainfall simulators, the sprays are swept laterally back and forth over the eroding area. Other experiments have been undertaken using static sprays that are interrupted intermittently.

In most field rainfall simulators, the rainfall is applied to the target as high intensity pulses. Such pulses are not common in natural rainfall and this leads to concern about how appropriate the results of experiments using such methods of applying rain are to determining erosion under natural conditions (Bower-Bower and Burt, 1989). Two major questions arise. Firstly, does the manner in which the rain is applied influence the susceptibility of the soil to erosion? Secondly, does the manner in which the rain is applied influence the transport processes operating in the rain-impacted flow environment to such an extent that the sediment transport rate is not directly related to the time averaged rainfall rate? In the past, the erosion processes were not understood well enough to develop a suitable analytical framework to answer this latter question. Now Eqs. 3.24-3.29 provide a basis by which data from appropriate experiments can be analysed to determine if pulsed rainfall has a unnatural effect on erosion by rain-impacted flow.

4.2.1 Experimental apparatus and method

A set of experiments secondary to the experiments described in Chapter 3 were undertaken to provide data for an analysis of the effect of pulsed rainfall on sediment transport by rain-impacted flow. In these experiments, 0.2 mm sand was used in 500 mm square and 75 mm deep target contained by a box installed in the downstream part of a small portable flume. As in the main experiments, flow over the target was produced by the combination of rain and a regulated flow of water input at the upstream end of the flume. Flow depth

was controlled by the height of a weir at the downstream end of the flume as in the main experiments. Similarly, a bleed of water was used to compensate for the extra inflow of water to the system when rain was applied and flow depths were monitored during rain using a pressure transducer.

The rains used in the experiments were produced by 1) a laboratory rainfall simulator using 2 overlapping Spraying Systems Veejet 80100 nozzles suspended about 1.8 m above the target, 2) a single Veejet 80100 nozzle suspended 3.2 m above the target, and 3) a single Spraying Systems Fuljet HH 30 WSQ nozzle suspended 3.2m above the target. The Veejet 80100 nozzles produce a fan spray pattern while the Fuljet HH 30 WSQ nozzles produce a square spray pattern. The Veejet 80100 nozzles are used in many simulators including the one used in the WEPP experiments. In the cases where the nozzles were suspended at 3.2 m, the nozzles were static. In the laboratory rainfall simulator, the nozzles were moved laterally back and forth in a controlled manner so as to apply a time averaged rainfall rate of about 100 mm h^{-1} when the nozzle pressure was 50 kPa (7.25 psi). The operational features of this simulator were described by Loch (1989). A nozzle pressure of 50 kPa (7.25 psi) was also used when the 80100 nozzle was mounted 3.2 m above the target while a 30 kPa (4.35 psi) pressure was used with the HH 30 WSQ nozzle.

The two nozzles in the laboratory simulator were 985 mm apart and, during experiments with this device, the target area was centred between the nozzles. In the case of the single 81000 nozzle, the target was centred 1m down along the fan line from the point immediately below the nozzle. This target position was maintained for the single HH 30 WSQ nozzle.

Average rainfall rates were measured at 16 points on a 4 by 4 grid in the 500 mm by 500 mm target area prior to a set of erosion tests with each type of rain. The grid spacing was 100 mm with a separation of 50 mm between the sides of the target area and the closest containers. Drop-size data were also collected at the 4 downstream points using a Distromet Distrometer. This is a commercial version of a device developed by Joss and Waldvogel (1967).

The target was eroded under each type of rain using 4 or 5 depths of flow within the range 4 mm - 8.5 mm. For each test under the laboratory simulator and the HH 30 WSQ nozzle, the rain was applied for 10 mins. For the single 80100 nozzle, the rain was applied for 3 mins. This 3 minute time limit

was used because applying the high instantaneous rainfall rates continuously from the 80100 nozzle for 10 mins could have produced a significantly different surface in terms of bed elevation to the other rainfalls. Duplicate tests were made for each depth. Prior to each test, the sand was screeded level and flow depth and velocity adjusted. A nominal flow velocity of 40 mm s^{-1} was used in the experiments but the actual flow velocities for each test were calculated from the flow depth and discharged data measured during a test.

4.2.2 Results

Table 4.4 shows the rainfall intensities measured at the 16 points on the target for each type of rain. Rainfall intensity was the most uniform under the laboratory simulator (dual oscillating 80100 nozzles) and the least uniform under the static 80100 nozzle. Because 0.2 mm sand travels, at most, only a matter of a few centimetres after being disturbed by a drop impact under the conditions that operate in these experiments, in terms of the sediment transported across the downstream boundary, the active zone (section 2.3) is close to that boundary. Consequently, the mean rainfall rates in the downstream area (row 4) are the ones used later in conjunction with the theory developed here to analyse the raindrop - flow interaction in these experiments.

Figure 4.8 shows the drop-size distributions measured using the Distromet Distrometer. These distributions result from applying a correction for the counting losses that result from variations in instrument dead-times associated with drops of various size (Kinnell, 1976) but the high intensities observed under the single 80100 nozzle tend to saturate the system. However, the losses under these circumstances can be assumed to be random with the result that the data shown in Fig. 4.8A are likely to be realistic. The coarser drop-size distribution observed for the 80100 nozzle is consistent with the visual impressions gained during the experiments.

Figure 4.9 shows the sediment discharge rates observed during the tests. The single 80100 nozzle produced the highest rates, the single HH 30 WSQ the lowest, and the laboratory simulator intermediate rates.

Table 4.4. Average rainfall rates measured at points on a 4 by 4 grid in the 500 mm by 500 mm target area during the experiments with rain produced by Spraying Systems Fuljet HH 30 WSQ and Veejet 80100 nozzles. 70 mm diameter containers were used to collect the rain. The grid spacing was 100 mm with a separation of 50 mm between the sides of the target area and the closest containers. Row 4 is the row closest to the downstream end of the target.

	Veejet 80100								HH30WSQ			
	single nozzle				lab. simulator				single nozzle			
Row	Column				Column				Column			
	A	B	C	D	A	B	C	D	A	B	C	D
	mm per hour											
1	1065	1065	777	433	80	80	83	78	52	57	64	70
2	929	827	618	357	84	86	86	81	41	47	52	55
3	722	720	546	309	96	93	97	89	33	35	40	44
4	641	599	394	245	91	96	94	96	25	28	31	34
mean for row 4	470				94				30			
	relative to mean for row 4											
1	2.27	2.27	1.65	0.92	0.85	0.85	0.88	0.83	1.73	1.90	2.13	2.33
2	1.98	1.76	1.31	0.76	0.89	0.91	0.91	0.86	1.37	1.57	1.73	1.83
3	1.54	1.53	1.16	0.66	1.02	0.99	1.03	0.95	1.10	1.17	1.33	1.47
4	1.36	1.27	0.84	0.52	0.97	1.02	1.00	1.02	0.83	0.93	1.03	1.13

FIG. 4.8

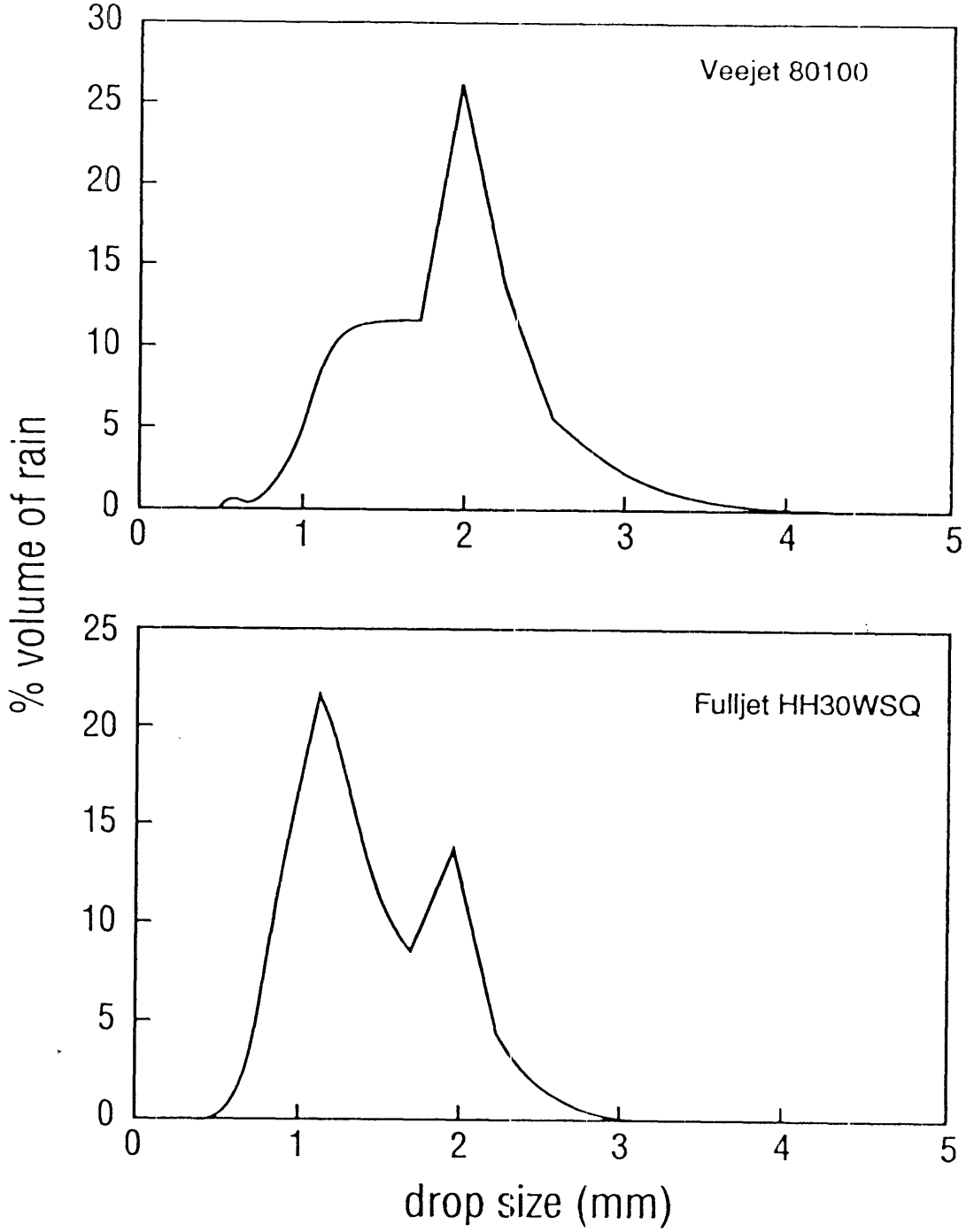

Figure 4.8. Drop size distributions at the downstream end of the 500 mm by 500 mm target area for Spraying Systems Veejet 80100 and Fulljet HH30WSQ nozzles measured using a Distromet Distrometer. Nozzle height was 3.2 m and the water pressures were 50 kPa and 30 kPa respectively.

FIG. 4.9

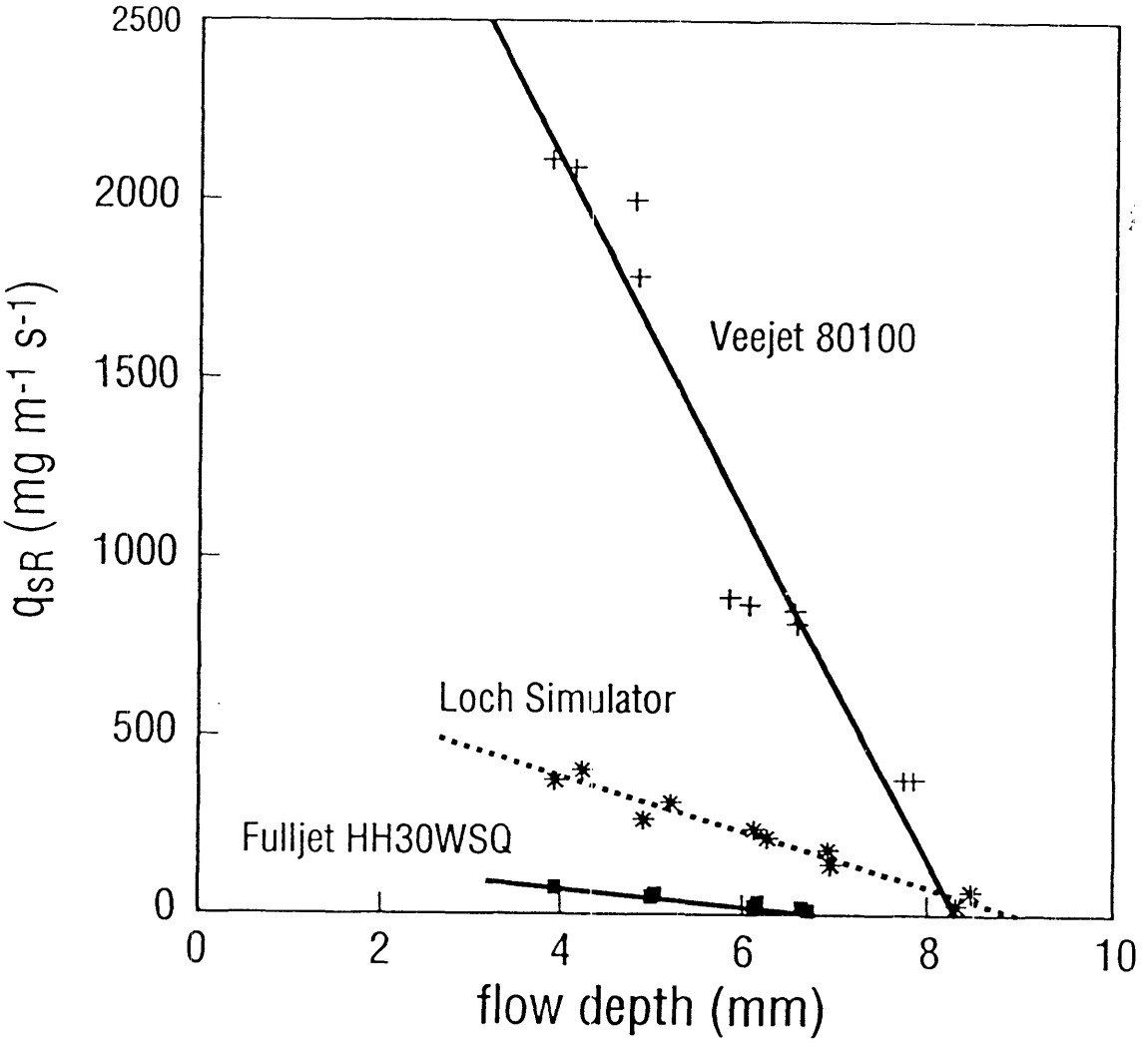

Figure 4.9. Sediment discharge rates (q_{sR}) produced by the various rains in the experiments with 0.2 mm sand when the nominal flow velocity was 40 mm s^{-1}.

4.2.3 Discussion

The effect of flow depth on the sediment discharge rates shown in Fig. 4.9 is linear as expected from Fig. 3.26 which resulted from rain with a drop size distribution not too dissimilar from those shown in Fig. 4.8. Figure 4.10 shows the effect of dividing the rates by the product of rainfall rate (R) and flow velocity (u). This figure shows q_{sR}/Ru or, because, from Eq. 3.28,

$$\frac{q_{sR}}{Ru} = k_s f[s,r] \qquad (4.18),$$

$k_s f[s,r]$ to be insensitive to the form by which the rain is applied using 80100 nozzles. Thus, without any further analysis, Fig. 4.10 shows that, at least for the 80100 nozzle, intermittency in rain application does not have a significant influence on the time averaged sediment transport rate when the susceptibility of the surface to erosion by rain-impacted flow remains constant. It should be noted that, because the laboratory simulator uses two overlapping 80100 nozzles 1.8m above the target, the instantaneous rainfall intensities under the laboratory rainfall simulator were considerably greater than those measured under the single 80100 nozzle. Thus the comparison between the single nozzle and the simulator involves more that just a reduction in the time rain is applied to the target.

Figure 4.10 also shows that q_{sR}/Ru varies between the 80100 and the HH 30 WSQ nozzles. From Eq. 4.18, it follows that the difference between the q_{sR}/Ru to flow depth relationships shown in Fig. 4.10 should result only from differences in the drop size characteristics of the two nozzles. Figure 4.11 shows the observed values of $k_s f[s,r]$ in relation to the values of $k_s f[s,r]$ predicted using Eqs. 3.25-3.29 in conjunction the drop size data shown in Fig. 4.8. Considering that the distrometer was not performing under ideal conditions, this result indicates the differences between the rainfall types considered can be accounted for by differences in average rainfall rate and raindrop size. Evidently, the answer to the question "Does the manner in which the rain is applied have a major influence the average sediment transport rate in the rain-impacted flow erosion environment when the susceptibility of the surface to erosion remains constant?" is no. The same answer may not be appropriate to the question "Does the manner in which the rain is applied

FIG. 4.10

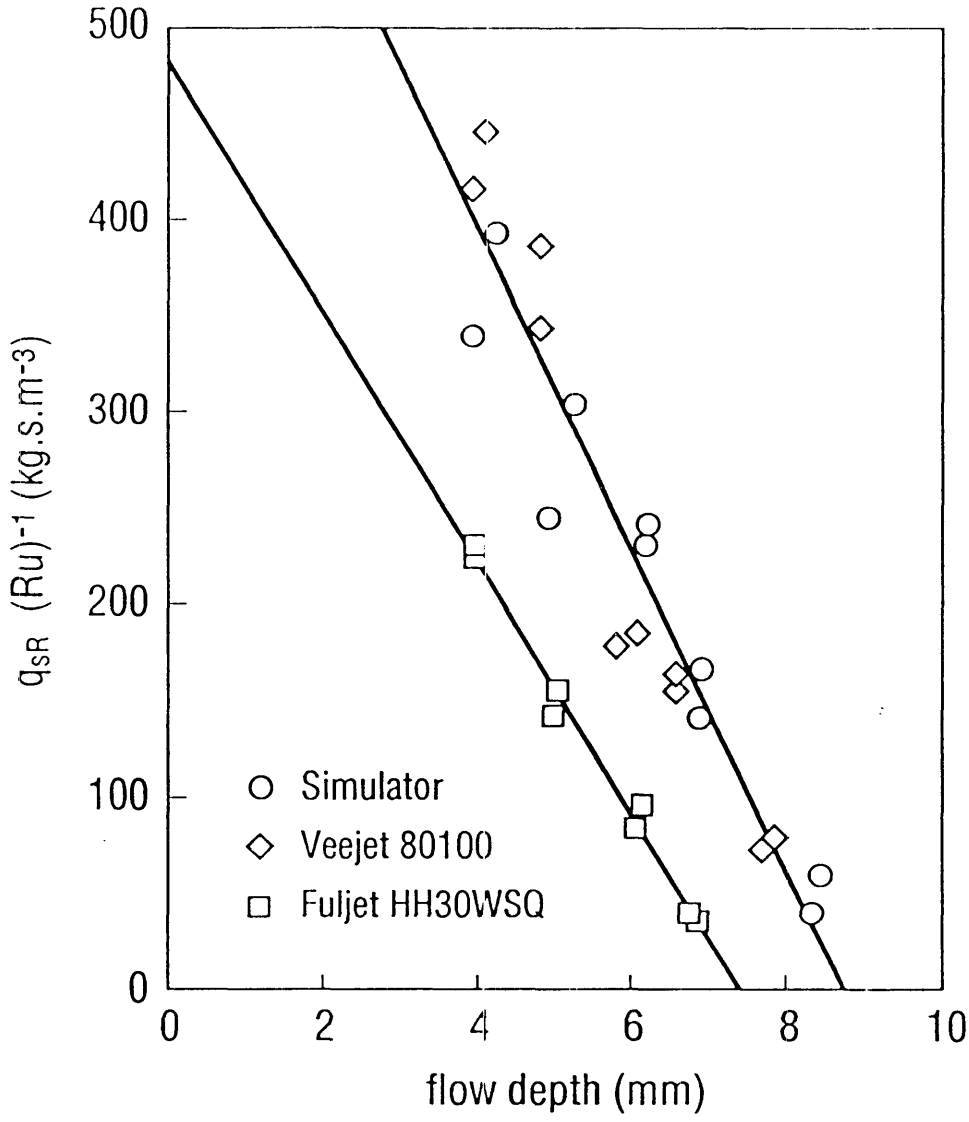

Figure 4.10. The relationship between the term q_{sR}/Ru and flow depth (h) for the various rains in the experiments with 0.2 mm sand.

FIG. 4.11

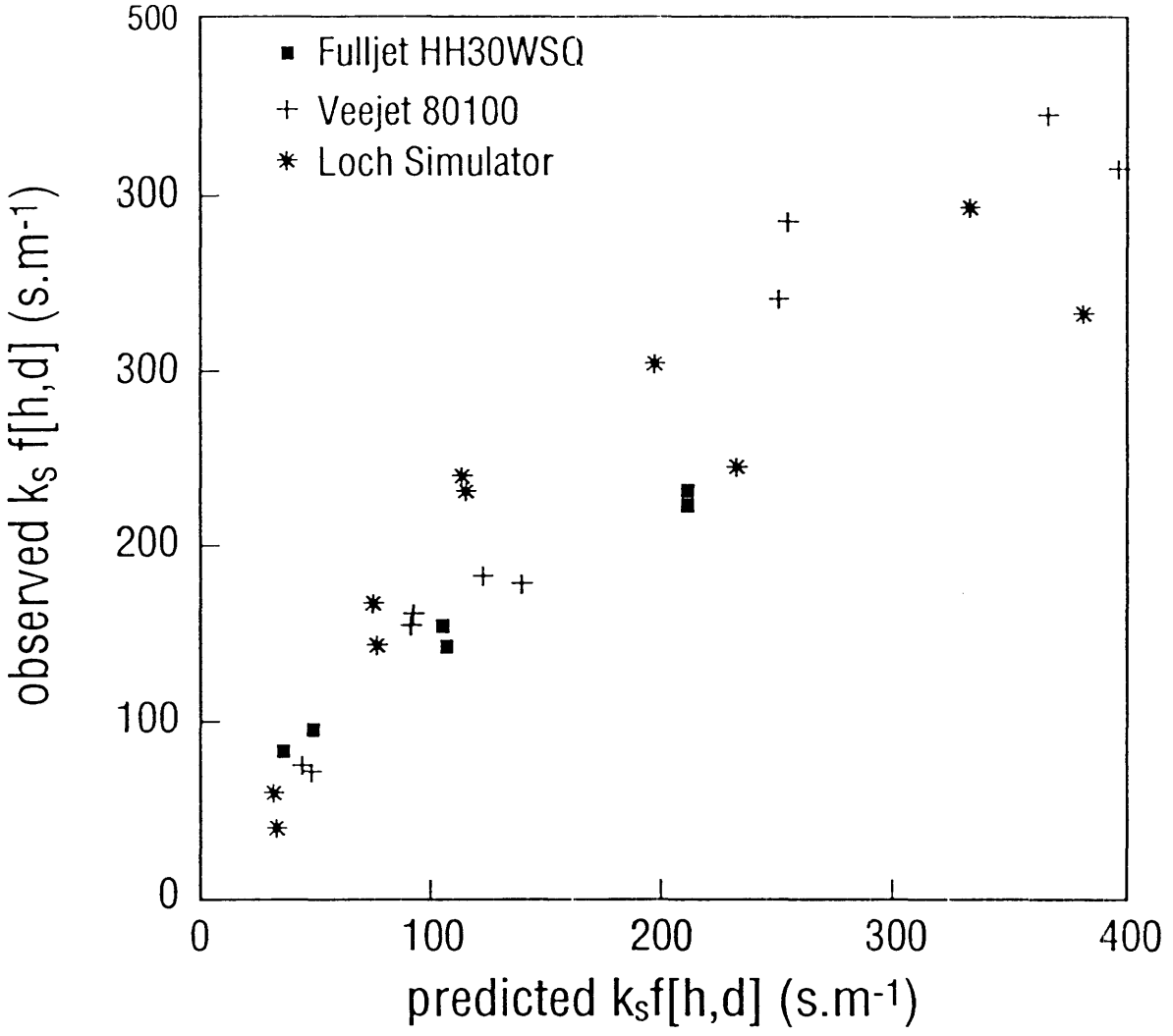

Figure 4.11. The relationship between the observed values of $k_s f[h,r]$ and those predicted from Eqs.3. 25-3.29 for 0.2 mm sand.

influence the susceptibility of the soil to erosion?". High energy pulses of rain may influence factors, such as aggregate breakdown and crust development, that affect the susceptibility of the soil to erosion differently to continuous rain. Consequently, concerns about the use of intermittent rainfall in soil erosion experiments remain.

CHAPTER 5

SUMMARY, CONCLUSIONS AND SUGGESTIONS FOR FURTHER STUDY

5.1 SUMMARY AND CONCLUSIONS

The downstream movement of soil particles that relies on repeated stimulation by raindrop impact is termed Raindrop Induced Flow Transport (RIFT). The theory for RIFT presented in this thesis relies on the observation that, after being lifted from the soil surface as a result of a drop impact, a particle travels a distance (x_p) downstream that depends on the time the particle remains suspended in the flow (t_p) and the velocity of the flow (u). The distance travelled controls the extent of a zone, called the active zone, in which all drop impacts cause soil material to pass across the boundary. As a result, the sediment transport rate (q_{sR}) across the boundary is given by the product of the frequency (f) of the drop impacts in this zone and the mass of material (D) each drop lifts into the flow. The sediment transport rate can be expressed as a function of rainfall intensity (R), raindrop size (d) particle size (p) and flow velocity by

$$q_{sR}\ (p,d) = \frac{6\ R_d\ t'_{pd}\ u\ D_{pd}}{\pi\ d^3} \qquad (2.20)$$

where t'_{pd} is the effective average duration of the suspension of p sized particles induced by the impact of drops of size d.

On soil surfaces, pre-detached particles are stored on the soil surface between impacts and, as a result, drop impacts may lift both pre-detached particles and particles from the soil matrix. Pre-detached particles sitting on the surface are lifted first and particles from the soil matrix are lifted only if there is excess energy left after this process. The pre-detached particles provide a degree of protection (H), with the result that

$$D_{pd} = H.D_{pd.D} + (1-H)D_{pd.M} \qquad (2.24)$$

where $D_{pd.D}$ is the value of D_{pd} obtained when the soil matrix is completely protected (i.e., H=1) and $D_{pd.M}$ is the value of D_{pd} obtained when no pre-detached material exists (i.e.,H=0). The need to store particles on the soil surface during the transport process results in the development of a layer of pre-detached particles on the soil surface. Through the use of a numerical model of the RIFT processes, the temporal and spatial variability of this layer is demonstrated in Section 2.4.

The effects of a number of the factors that influence RIFT are examined experimentally in Chapter 3. Available data, together with new data collected during this study, confirm that Eq. 2.20 can account for effects of R and u on q_{sR}. These data also show that q_{sR} is influenced by particle size, density and flow depth (h). Apart from drop size and particle size, factors such as drop velocity, drop shape, particle density, and flow depth influence D_{pd} and t'_{pd}. The data collected during the study show that,

$$D_{pd}t'_{pd} = k_0(1 - \beta h) \qquad \text{for } h_1<h<h_2 \quad (3.5)$$

where $h_1 \approx 4$ mm and $h_2 \approx 3d$, k_0 is the intercept on the "y" axis projected by the linear equation

$$D_{pd}t'_{pd} = k_0 - b_2h \qquad (3.6),$$

and β is the inverse of the projected intercept on the "x" axis. Both β and k_0 vary with drop size and velocity but β varies independently of the characteristics of the eroding surface. k_0 is influenced by both the drop and the surface characteristics and k_0 decreases in value with particle fall velocity to a power less than 0.5 when particle size varies.

In this study, coal was used to examine the movement of particles of a density similar to that of aggregates. The experiments showed that the values of q_{sR} for coal particles greatly exceeded the values for sand with a similar particle fall velocity. Also, the effect of particle density could not be determined simply through Eq. 3.5 because, for 5.1 mm drops, the lower limit (h_1) for coal particles greatly exceeded that observed for sand. Despite this, Eq. 3.5 is valid for erosion of soil (as opposed to sand and coal) surfaces by rain-impacted flows where a wide range of particle size and density are present.

It follows from the combination of Eqs. 2.20 and 3.5 that the effects of rain (r), flow and soil (s) on q_{sR} can be represented by an equation of the form

$$q_{sR}[s,r] = k_s \, R \, u \, f[h,r] \qquad (3.21)$$

where k_s is the susceptibility of the soil to erosion by rain-impacted flow and $f[h,r]$ is a function that accounts for the interaction between raindrop size and flow depth. Analysis of the data from the experiments presented here, together with the data from Moss and Green (1983), indicates that raindrop size has a non-significant influence on q_{sR} when medium-to-large drops travelling at or close to their terminal velocities impact flows shallower than about 4 mm. Evidently, this effect results from the water surface restricting the height to which particles are lifted in the flow when these high energy drops impact shallow flow because drop size influences q_{sR} when small drops travelling at terminal velocity, and medium-to-large drops travelling at subterminal velocity, impact flows shallower than 4 mm. On the basis of the apparent constraint placed on q_{sR} by the height of the water surface, the q_{sR}-h relationship observed for 5.1 mm drops travelling at terminal velocity,

$$q_{sR}[s,r] = 0.001553 \, k_s \, R \, u \, h \exp(5.7975 - 0.1881h),$$

provides a mechanism for determining the upper limit of q_{sR} for flows shallower than about 20 mm. The above equation results from

$$k_s f[h,d] = h \exp(5.7975 - 0.1881h) \qquad (3.26a)$$

and the observation that, for 0.2 mm sand used in the experiments, k_s = 644 kg.s m^{-3} (Table 3.7).

In that, at some critical depth (h_c), the $f[h,d]$ to h relationship departs from Eq. 3.26a, Eq. 3.26a is applies when $h \leq h_c$, and, for 0.2 mm sand,

$$k_s f[h,d] = h \exp(5.7975 - 0.1881h_c - b'_d(h-h_c)) \qquad (3.26b)$$

where

$$b'_d = \exp(0.77749 - 0.48251\ d) \qquad (3.27)$$

applies when $h<h_c$. Together, Eqs. 3.21, 3.26 and 3.27 provide a mechanism for estimating the effect of drop size - flow depth interaction for rain with non-uniform drop-size distributions, and a mechanism for separating the erosivity and erodibility components in erosion by rain-impacted flow. Using this mechanism, the assumption that the time averaged effect of rainfall on sediment transport by rain-impacted flow is independent of whether rain is applied as a pulse, as often the case with field rainfall simulators, or applied as a continuous stream, as in the case of natural rainfall, was found to be valid (Section 4.2). However, the effect of pulsed rainfall on variations in the susceptibility of surfaces to erosion lies outside the scope of this study.

While factors such as flow depth (h) and velocity (u) directly affect q_{sR}, they are seldom measured. It is well known that sediment discharge is given by the product of flow discharge (q_w) and sediment concentration (c). Thus

$$q_{sR} = q_w\ c_R \qquad (4.5)$$

where c_R is the sediment concentration resulting from the raindrops impacting the flow. Since flow discharge is the product of flow depth and velocity, it follows from Eq. 3.21 that

$$c_R[s,r] = k_s\ R\ f[h,r]\ h^{-1} \qquad (4.6)$$

and

$$q_{sR} = k_s\ q_w\ R\ f[h,r]\ h^{-1} \qquad (4.7).$$

Considering q_{sR} in terms of flow discharge thus eliminates the need to consider flow velocity but the effect of flow depth remains to be accounted for. However, it is also well known that slope gradient (S) influences flow depth and velocity and, as a result, Eq. 4.7 can be rewritten as

$$q_{sR} = k_1\ q_w\ R\ f[S] \qquad (4.8)$$

where $f[S]$ is a function that accounts for the effect of slope gradient on q_{sR} and k_1 is a coefficient influenced by variations in soil characteristics and also by variations in flow depth that are not accounted for directly by $f[S]$. Analysis of data from Meyer and Harmon (1989) shows that, for S<30 %,

$$f[S] = S \qquad (4.9)$$

but, as a result of the departures from Eq. 4.9 that were implied by theory and observed in other experiments, other functions may be more appropriate.

Equation 4.8 is comparable to a widely used model that uses R^2 rather than R q_w, and K_i rather than k_1. Analysis of 18 cropland soils used in the USDA Water Erosion Prediction Project (WEPP) in terms of the two models indicates that the susceptibility of some soils to erosion by rain-impacted flow may differ substantially from the values used in WEPP (Section 4.1).

5.2 SUGGESTIONS FOR FURTHER STUDY

5.2.1 Modelling the dynamic depositional layer in large areas

In Chapter 2 (Section 2.4), a computer program for modelling the process of particle uplift, downstream movement and deposition was used to demonstrate the influence of particle and flow factors on the development of a layer of pre-detached particles on the soil surface. This layer, hereafter referred to as the Dynamic Depositional Layer (DDL), results from the need for RIFT to store particles on the soil surface between raindrop impacts when particles are not being entrained by the flow. This layer is important in controlling sediment transport when RIFT operates. Consequently, there is a need to model the development and functions of the DDL over large areas if accurate predictive models of interrill and sheet erosion are to be developed. As noted in Chapter 2, the enormity of the task of keeping track of the effect of individual drop impacts over large areas makes the use of modelling concepts described Section 2.4 impractical for field sized areas. An alternative approach is suggested here.

The concepts that are central to this approach are:

1) Material entering any arbitrary element is deposited on the soil surface before being moved downstream by subsequent drop impacts. Consequently, the deposition event and the subsequent uplift event can be treated separately.

2) Material entering an element is deposited on the soil surface over an area that varies with the distance particles travel after being disturbed by a drop impact. For any given particle, this distance can be estimated from the height the particle is lifted, particle fall velocity and flow velocity.

3) Likewise, material leaving an element comes from a zone, the active zone, the area of which varies with the distance particles travel after being disturbed by drop impact.

4) The protective effect of the DDL in an element is absolute (H=1) when the mass of material in the DDL in the active zone associated with any particle is greater or equal to the mass RIFT can transport from that zone when the particles are held to the surface by only gravity or a little more than gravity. Otherwise, the protective effect varies directly with the ratio of the mass of the DDL in the active zone and the maximum mass that can be transported from the active zone in the period of time being considered.

These concepts allow the mass of material being deposited to the DDL during an increment in time to be compared with the capacity of RIFT to transport that material out of the element in order to calculate the protective effect of the DDL. Once this protective effect (H) has been calculated, and given an estimate of the $D_{pd.M}$-to-$D_{pd.D}$ ratio, it is possible to calculate the mass ($q_{so}[p]$) of p sized particles being transported across the downstream boundary of any element from

$$q_{so}[p] = q_{soD}[p] + q_{soM}[p] \qquad (5.1)$$

where

$$q_{soD}[p] = H\ P_{pD}\ k_p\ R\ u\ f[h,r]\ W_f \qquad (5.2)$$

represents the mass coming from the DDL,

$$q_{soM}[p] = f_p\ (1-H)\ P_{pM}\ k_p\ R\ u\ f[h,r]\ W_f \qquad (5.3)$$

represents the mass coming from the soil matrix, P_{pD} and P_{pM} are the proportions of p sized particles in the DDL and soil matrix materials respectively, f_p is the $D_{pd.M}$-to-$D_{pd.D}$ ratio, and the other factors are as defined previously. The total mass of the material transported across the boundary can be calculated by integrating Eq. 5.1 with respect to p.

A computer model that demonstrates the use of these concepts is given in Appendix III. In the computer model, flow over a plane is represented by major elements in which flow depth and velocity remain uniform in space and time. The computer model calculates erosion, deposition, and re-detachment of deposited particles resulting from raindrop impacting flows in small elements lying within these major elements. The model commences by calculating the mass of material eroded from the most upstream element. This material then enters the next downstream element, and is deposited to the dynamic depositional layer (DDL) in a manner that depends on flow depth, flow velocity and particle fall velocity. In the model, the data from the experiments in Chapter 3 are used to provide the estimates of the capacity of RIFT to transport particles from the element and this is used to calculate H. Once H has been determined, it is used to calculate the masses of the particles transported from both the DDL and the soil matrix within the element, and this material then becomes the input to the next downstream element. Because the model works progressively downstream from the most upstream element, it operates as a "steady-state" model. However, the concepts used to determine H can be applied in non-steady state models where the mass balances can be determined both temporally and spatially.

Table 5.1 shows some of the results achieved using the model on a 40 m long plane covered by an arbitrary sandy soil under 50 mm h^{-1} rain having the same drop-size characteristics as produced by Veejet 80100 nozzles. Flow depths and velocities vary in an arbitrary manner downstream along the plane and the simulation uses f_p=0.01. A full set of results is included at the latter part of Appendix III.

The particle-size distributions produced by the simulation show the DDL becoming progressively coarser with distance down the plane. It changes rapidly from the matrix distribution at the upstream end of the plane but the rate of change decreases as the distance down the plane increases. The

Table 5.1. Spatial variations in particle size distribution (expressed proportions of the total mass) and the protective effect of the DDL (H) produced by the model in Appendix III

PARTICLE SIZE DISTRIBUTIONS

		Distance Downslope				
		0.5m	1.5m	7m	19m	40m
p	Matrix	DDL				
(mm)		(proportion of total mass)				
0.02	0.050	0.000023	0.000023	0.000016	0.000011	0.000008
0.04	0.020	0.000026	0.000026	0.000017	0.000012	0.000008
0.06	0.020	0.000049	0.000048	0.000032	0.000022	0.000015
0.08	0.050	0.000199	0.000197	0.000129	0.000089	0.000062
0.10	0.070	0.000418	0.000413	0.000271	0.000187	0.000129
0.20	0.500	0.012977	0.012808	0.008352	0.005734	0.003961
0.40	0.200	0.062504	0.056868	0.030218	0.019822	0.013348
0.80	0.070	0.795278	0.817091	0.901476	0.939363	0.961215
1.00	0.019	0.128246	0.112270	0.059349	0.034667	0.021191
2.00	0.001	0.000278	0.000256	0.000140	0.000092	0.000062
Flow Depth (mm)		0.01	0.5	1.5	2.5	3.0
Flow vel. ($mm\ s^{-1}$)		5.0	10.0	40.0	110.0	160.0
H		0.491	0.494	0.596	0.681	0.755
Sed Disch ($kg\ m^{-1}\ s^{-1}$)		5.51e-8	5.03e-6	5.83e-5	2.33e-4	5.24e-4

protective effect of the DDL follows a similarly pattern, H increasing rapidly with distance at the upstream end and less rapidly at the down stream end. The rate soil material is transported across the arbitrary boundaries associated with each major element increases downstream along the plane as a result of the increases in H and particle travel distance as flow depth and velocity increase along the direction of flow.

These above results are as expected but they only provide a demonstration of how the principles discussed above can be used to model the spatial development of the DDL and its effect on erosion. A more realistic set of rain, flow and soil conditions would be necessary to test its real ability to model RIFT at a field scale. It is likely that some of the assumptions used currently need modification. For example, it would be best if the downstream length of the elements used was equal to the minimum distance of particle travel in a major element. The current practice of setting the element length to a fixed proportion of the major element length will cause variations in the results depending on the length of the major element and proportion selected. How much a departure from the real result is produced warrants some investigation. A more accurate determination of particle travel distance may be necessary. Currently, Rubey's (1933) formula is used to calculate particle fall velocity but other more accurate formulae may be more appropriate. Also, turbulence and the time taken for the particles to be rise from the bed are not considered currently in the model. The assumption that particles are distributed evenly throughout the depth of flow may also not be true, particularly when flow depths increase beyond 3 drop diameters.

Although some of the assumptions used currently in the model may need to be modified, the effects of entrainment by flow on the DDL outlined in Chapter 2 are not included in the model. The inclusion of these effects, and the ability to account for entrainment of material from the soil matrix, is necessary if the model is to adequately account for temporal and spatial variations in erosion by rain-impacted flows. Obviously, this is an area for further study.

5.2.2 The effect of slope gradient on interrill erosion

The practical model of interrill erosion developed in Chapter 4 includes

slope gradient (S) as one of its terms. The term was included to account for the effect of variations in flow depth that result from changes in slope gradient. The direct use of S results from an analysis (Fig. 4.2) of the data of Meyer and Harmon (1989) but there is evidence that indicates that this relationship is not applicable at high and very low slope gradients. At a zero gradient, the function used results in c=0 when, in reality c can exceed zero when S=0. Likewise, the analysis of the data used by Liebenow *et al.* (1990) in Chapter 4 indicated that Eq. 4.9 overestimates the effect of slope at high slope gradients. The effect of slope at low slope gradients needs to be clarified. Experiments by Cummings (1981), where 0.9 m long planes of soil were eroded under the same rain producing system as used here in Chapter 3, indicate that, when slope gradients are less than 25 %, the effect of slope gradient in Eq. 4.10 may be expressed by

$$f[S] = a_S + b_S S \qquad (5.4)$$

where a_S and b_S are empirical coefficients that vary between soils. The approach adopted by Liebenow *et al.* (1990), where coefficients such as these have values that are considered common to all soils, may not be totally realistic. Also, it has been shown (Kinnell, 1985) that, on longer planes (e.g., 3 m), Eq. 5.4 should be replaced by

$$f[S] = \exp (a_S + b_S S) \qquad (5.5).$$

In this situation, variations in entrainment by flow contribute to the effect of slope on erosion. Also entrainment by flow needs to be cosidered when flow conditions are conducive to the development of rills in previously unrilled interrill areas on shorter steep slopes. In addition, changes between detachment limiting and transport limiting conditions may occur as slope gradient increases without rilling (Foster, 1990). With the effect of slope gradient on erosion being influenced by a number of factors, there is a need to develop functions that are able to account for interactions between slope gradient, slope length and soil characteristics within models, such as Eq. 4.8, which include an ability to account for surface-water flow on erosion in sheet and interrill erosion areas.

5.2.3 An alternative to the EI_{30} index

As knowledge of rainfall erosion processes grows, opportunities are presented to examine and model erosion processes better at various levels. Here, in this thesis, consideration has been given to modelling the effect of individual drop impacts (Section 2.4), a finite difference approach (Section 5.1), and the level used in the USDA Water Erosion Prediction Project (Sections 4.1 and 5.2.3). The Water Erosion Prediction Project (WEPP) was inaugurated to develop methods of predicting soil erosion that are more process orientated than the Universal Soil Loss Equation (USLE). Despite its promise of greater applicability, WEPP has yet to replace the USLE or the latest version of it, the Revised Universal Soil Loss Equation (RUSLE), because some aspects of the project have yet to be completed. The predictive erosion models being developed within WEPP also require data sets that are available in the USA but which are not readily available elsewhere. This may preclude the use the WEPP models in many parts of the world. Consequently, the widespread use of the USLE and its upgrade, RUSLE, can be expected to continue even when the USDA formally adopts the approaches developed in WEPP as the basis for decision making on soil conservation issues in the USA. While RUSLE attempts to eliminate some of the shortfalls of the USLE, the product of total storm rainfall energy (E) and the maximum 30 minute rainfall intensity (I_{30}) remains as the parameter used to estimate the erosive potential of rainfall. Just as the square of rainfall intensity fails to account for the effect of variations in soil infiltration rate in WEPP, so too does the EI_{30} index in the USLE and RUSLE. Admittedly, the USLE and RUSLE include soil permeability in the nomogram for calculating erodibility but, in terms of the erosion processes, variations in the soil's infiltration rate do not influence erodibility. They influence the erosive stress. Also, no major provision is made within the USLE and RUSLE to account for variations in antecedent moisture conditions which can have a substantial effect on the erosion caused by particular rain storms.

Just as consideration of the product of flow discharge and sediment concentration provided an alternative interrill erosion model to the one currently used in WEPP, so too does this product provide an alternative to the EI_{30} index in the USLE and RUSLE. Not surprisingly, sediment concentrations in the runoff from soil loss plots such as used to develop the USLE vary with rainfall intensity when slope gradients are low (Doty and Carter, 1965). Thus

the product of flow discharge and rainfall intensity, or alternatively, the rate of expenditure of rainfall energy, which is highly correlated with rainfall intensity (Kinnell, 1973), can provide a measure of the erosive stress in areas dominated by sheet erosion (Kinnell, 1985). Analysis of data from plots which readily rill (Armstrong, 1990) indicates that this product is also useful when rills are present on an eroding area. The reason for this appears to be the result of the correlation between runoff rate and rainfall rate, particularly on soil where infiltration rates are low, and the correlation between rainfall intensity and the rate of expenditure of rainfall kinetic energy. Evidently, the product of flow discharge, or its surrogate, the excess rainfall rate (Kinnell, 1983, 1985), and the rate of expenditure of rainfall kinetic energy has a no lesser potential to account for the erosivness of a rainfall event than the EI_{30} index while also having the ability to account for antecedent moisture conditions which are important in prediction erosion produced by individual storms. It is probable that, while soil erodibilities would need to be re-evaluated if EI_{30} were replaced by this product, many of the algorithms and procedures for determining the effect factors, such as vegetative cover and changes in organic matter, that are currently part of the USLE and RUSLE could be retained. If so, then such a model could perhaps fill the void between the USLE and WEPP in many parts of the world.

5.4 CONCLUDING REMARKS

In addition to providing alternative or improved methods for predicting soil erosion, the work reported here has produced some unexpected results. In particular, the effect of particle fall velocity depends on whether the change in fall velocity results from a change in particle size or density (Section 3.4). This result requires further investigation if the differential movement of primary particles and aggregates is to be accounted for well. There may be a need for this when predicting the movement of nutrient and pollutants that are sorbed into the clay material present in aggregates. Except for a few soil surfaces, the materials studied were uniform in size. The effects of mixtures of various sized particles on sediment transport by RIFT are not known and, if studied, may show that the assumption that the effect of a particles of a given size can be treated in isolation from other particles of different size (used in Section 5.1) over-simplifies reality. There are many other aspects of

erosion by rain-impacted flow that the work here may provide a focus for a new or alternative approach. Those new or alternative approaches are matters for future research and development.